



Article

Black TiO₂ and Oxygen Vacancies: Unraveling the Role in the Thermal Anatase-to-Rutile Transformation

Mattia Allieta ^{1,*}, Mauro Coduri ^{2,3} and Alberto Naldoni ⁴ ¹ Ronin Institute Montclair, Montclair, NJ 07043, USA² Department of Chemistry, University of Pavia, Via Taramelli 16, 27100 Pavia, Italy; mauro.coduri@unipv.it³ National Inter-University Consortium for Materials Science and Technology (INSTM), Via G. Giusti 9, 50121 Florence, Italy⁴ Department of Chemistry and NIS Centre, University of Torino, Via Pietro Giuria 7, 10125 Torino, Italy; alberto.naldoni@unito.it

* Correspondence: mattia.allieta@gmail.com

Abstract: Understanding the role of oxygen vacancies in the phase transformation of metal oxide nanomaterials is fundamental to design more efficient opto-electronic devices for a variety of applications, including sensing, spintronics, photocatalysis, and photo-electrochemistry. However, the structural mechanisms behind the phase transformation in reducible oxides remain poorly described. Here, we compare P25 and black TiO₂ during the thermal anatase-to-rutile transformation using in situ synchrotron powder diffraction. The precise measurement of the phase fractions, unit cell parameters, and Ti-O bond sheds light on the phase transformation dynamics. Notably, we observe distinct temperature-dependent shifts in the relative phase fractions of anatase and rutile in both materials highlighting the role of the oxygen vacancy in promoting the phase transformation. We employ bond valence concepts for structural modeling, revealing unique trends in temperature evolution of Ti-O distances of black rutile, confirming that this TiO₂ phase is preferentially reduced over anatase. These findings not only enhance our understanding of phase transitions in TiO₂ but also open new ways for the design of advanced photocatalytic materials through targeted phase control.

Keywords: TiO₂; P25; black TiO₂; renewable energy photocatalysis; Rietveld refinement



Citation: Allieta, M.; Coduri, M.; Naldoni, A. Black TiO₂ and Oxygen Vacancies: Unraveling the Role in the Thermal Anatase-to-Rutile Transformation. *Appl. Nano* **2024**, *5*, 72–83. <https://doi.org/10.3390/applnano5020007>

Academic Editor: Francesco Enrichi

Received: 18 March 2024

Revised: 16 April 2024

Accepted: 17 April 2024

Published: 3 May 2024



Copyright: © 2024 by the authors. Licensee MDPI, Basel, Switzerland. This article is an open access article distributed under the terms and conditions of the Creative Commons Attribution (CC BY) license (<https://creativecommons.org/licenses/by/4.0/>).

1. Introduction

In the ever-evolving landscape of materials science, nanostructured titanium dioxide (TiO₂) stands out as a material of paramount importance due to its technological applications ranging from sensors and solar cells to energy conversion and hydrogen production [1,2]. In particular, in the last few decades, the emerging interest in the reduced black TiO₂ has revolutionized the field of photocatalysis with its outstanding visible light absorption and charge separation efficiency [3–7].

TiO₂ exists in various polymorphic forms, with anatase and rutile being the primary focus due to their activities under UV irradiation [8,9]. The thermal anatase-to-rutile transition is not just a mere phase transformation but a gateway to understanding and harnessing the true potential of TiO₂ in various applications [9]. However, the criticality of the anatase-to-rutile transition remains a subject of intensive debate, primarily due to the varying transition temperatures and its reconstructive atom bond mechanism influenced by nanocrystal size, impurities, annealing temperature, and synthesis conditions [9,10]. As an example, very recently advanced characterization techniques such as ATR-FTIR, EELS, EFTEM imaging, XPS, Raman spectroscopy, and DRIFTS have confirmed the successful doping of the TiO₂ nanoparticles with nitrogen, phosphorus, and carbon [11]. This doping significantly enhanced the photocatalytic properties of the nanoparticles, as evidenced by their ability to inhibit electron-hole recombination by 7.3 times compared to the standard P25 photocatalyst. The doped nanoparticles resisted the anatase-to-rutile phase

transformation, maintaining their anatase structure even after a calcination temperature of 700 °C [11]. On the other hand, the modification of the TiO₂ structure to form reduced black TiO₂ by oxygen vacancies not only narrows the band gap but also potentially alters the dynamics of the anatase-to-rutile transition [12]. Depending on the TiO₂ precursor used for the synthesis, the oxygen vacancies could promote or prevent the fusion of neighboring anatase nanocrystals by inhibiting the anatase-to-rutile transformation. In particular, the surface-adsorbed fluoride ions play a crucial role in the formation of surface oxygen vacancies upon calcination [13]. These vacancies contribute to the high thermal stability of the TiO₂-NSs (nanosheets) and prevent the early phase transition from anatase to rutile TiO₂, allowing the material to retain its high photocatalytic activity at higher temperatures [13].

Despite the extensive literature on the TiO₂ phase transformation, a significant gap exists in understanding the temperature dependence of unit cell parameters and microstructure. Previous studies have predominantly used ex situ powder X-ray diffraction (XRD) to determine these parameters [14], but this may yield less reliable outcomes due to the loss of thermally triggered lattice features upon cooling [10]. On the other hand, in situ XRD methods offer a more accurate picture of phase transformation and the available studies on the thermal behavior of anatase in air have indicated a linear expansion of unit cell parameters with increasing temperature [15]. In contrast, Hummer and coworkers demonstrated that polynomial models are more effective than linear ones for characterizing the changes in the *a* and *c* axes [14]. However, these investigations are confined to temperatures below the phase transition threshold, thereby limiting insights into lattice alterations during phase transformation. Recently, an in situ powder diffraction study with Cu source on a commercial P25 sample, a 85:15 mixture of anatase and rutile nanoparticles (NPs), revealed really unusual properties across the anatase-to-rutile phase transition [10]. Notably, an average negative thermal expansion of the anatase *c*-axis was observed accompanied by the decrease in particle size with increasing temperature in the temperature range of $673 \leq T \leq 973$ K [10].

This finding not only profoundly contradicts the previously reported linear behavior but also adds complexity to the understanding of the TiO₂ structure leaving the issue of structure characterization wide open. This rather puzzling scenario underscores the need for more detailed studies in order to offer the most thorough understanding of this transformation.

The present study aims to embark on a comprehensive investigation of the anatase-to-rutile transition in both conventional P25 and black TiO₂ samples, employing in situ temperature-dependent high-resolution synchrotron powder diffraction. Thanks to high resolution in reciprocal space, the intrinsic narrow instrument resolution function, and an intense monochromatic photon flux offered uniquely by synchrotron radiation facilities, this approach enabled us to analyze the evolution of structural parameters (e.g., unit cell parameters) more accurately than conventional powder diffractometer providing a broad description of the phase transition occurring in transition metal oxides [16].

Through correlating our findings with the structural stability, mechanism, and progression of the transformation, we aim to bridge the existing knowledge gap and elucidate the critical role of this transformation. Moreover, this study also emphasizes the need to explore the properties and applications of reduced black TiO₂. The advent of black TiO₂, with its narrowed band gap and enhanced visible light catalytic performance, represents a significant advancement in photocatalysis. This variant of TiO₂, which emerged from hydrogenation strategies, exhibits potential for greater light utilization efficiency and quantum efficiency, addressing the limitations of traditional TiO₂ in harnessing solar energy. This paper aims to provide new insights into the anatase-to-rutile phase transition of TiO₂, particularly focusing on the evolution of the P25 TiO₂ sample across this thermal-induced transition. Through shedding light on the structural and microstructural changes during this transition, this study will contribute to a better understanding of TiO₂ photocatalytic efficiency, particularly emphasizing the role of reduced black TiO₂.

2. Experimental/Calculation Techniques

Degussa P25 was used as the raw TiO₂ material while black TiO₂ was produced by the procedure described in [4]. Commercial amorphous TiO₂ powder (NanoActive[®]; NanoScale Co., Manhattan, KS, USA) was initially treated under vacuum (10⁻⁵ mbar) and then heated at 200 °C under flowing O₂ for 1 h, to oxidize and favor the desorption of molecular species adsorbed onto the surface of the metal oxide. After the sample reached RT, the obtained sample was subjected to a reduction in H₂ flow at 500 °C for 1 h. All thermal treatments were carried out using a heating rate of 10 °C/min. The sample cooling was performed under inert gas flow by placing the reactor outside the furnace with a cooling rate of ~50 °C/min

High-resolution synchrotron powder diffraction experiments were performed at the High-Resolution Powder Diffraction beamline (former ID31) of the European Synchrotron Radiation Facility (ESRF), working in transmission geometry and employing the setup equipped with crystal analyzers [17]. The wavelength of the incident beam was set to $\lambda = 0.30988$ Å. 31 patterns in the $0 \leq 2\theta \leq 50^\circ$ range data were collected for about 1 h counting time between 93 K and 993 K. Both the samples were cooled down to 93 K using an N₂ gas stream, while from 303 K an air blower was employed to achieve the highest temperature. It should be noted that the powders within the capillary were completely sealed off from the N₂, ensuring that they did not come into contact with the gas and thus preventing any direct interaction with the material.

Data at each temperature were analyzed with the Rietveld method. Structural refinements were performed through the GSAS program [18] by implementing simultaneously the anatase tetragonal model of the $I4_1/amd$ space group [19] and the rutile tetragonal model of the $P4_2/mnm$ space group [20]. During the refinement, the background was subtracted using shifted Chebyshev polynomials and the diffraction peak profiles were fitted with a modified pseudo-Voigt function [18]. In the last calculation cycles, all the parameters were refined including the unit cell parameters, atomic positional degrees of freedom, isotropic thermal parameters, background, diffractometer zero-point, and line profile parameters together with the phase fraction (%) of the anatase and rutile phases. It should be noted that we did not refine the occupation factor related to oxygen in the anatase and rutile phases of the black TiO₂ sample. Within this model, all the occupation factors were set to unity and, hence, any contribution of the H₂ reduction process to TiO₂ structural evolution upon increasing T was accommodated in the refined parameter of the structural model. This approach helps prevent potential correlations between structural parameters.

According to GSAS formalism [18], the estimation of the particle size dimension was determined by the relation $D = 18,000 K\lambda/\pi L_x$, where $K = 0.9$ is the Scherrer constant and L_x is the refined Lorentzian broadening parameter. This approach, despite being based on empirical functions and on the assumption of spherical monodisperse particles, takes into account all the observed reflections and separates the finite size effect from microstrain, like a conventional Williamson–Hall approach. Whilst the crystal size is more likely to be a wide distribution, the values extracted here can be taken as reference values to monitor the evolution with T . Eventually, owing to the extremely high instrumental resolution, it is possible to resolve limited coherence lengths even larger than 100 nm, which would be unreliable using laboratory instruments.

The thermal expansion coefficient $\alpha_{\varphi,T}$ (K⁻¹) was determined from the relation $\alpha_{\varphi,T} = \frac{1}{\varphi_{(T-\Delta T)}} \frac{\varphi_T - \varphi_{(T-\Delta T)}}{\Delta T}$ where φ_T stands for a and c axis determined at each T of anatase and rutile phases in P25 and black TiO₂ samples.

3. Results and Discussion

Figure 1a–d show the powder diffraction patterns related to P25 and black samples at selected T . All the diffractograms show the presence of both anatase and rutile and, within the resolution of our measurements, we did not detect any spurious crystalline phases at each T . At the lowest T , P25 is composed of 87.3% of the anatase phase and 12.7% of the rutile phase, whereas at $T = 993$ K it is composed of 55.1%/44.9%, respectively. The black

sample shows a similar composition at $T = 93$ K (86.7% anatase, 13.3% rutile), whereas at $T = 993$ K rutile increases up to 68.6%. The overall temperature evolution of the relative phase weight fraction is presented in Figure 2a. Phase transformation from anatase-to-rutile phase was detected in both the samples. In the P25 and black samples, the transition began at about $T = 843$ K and $T = 723$ K, respectively.

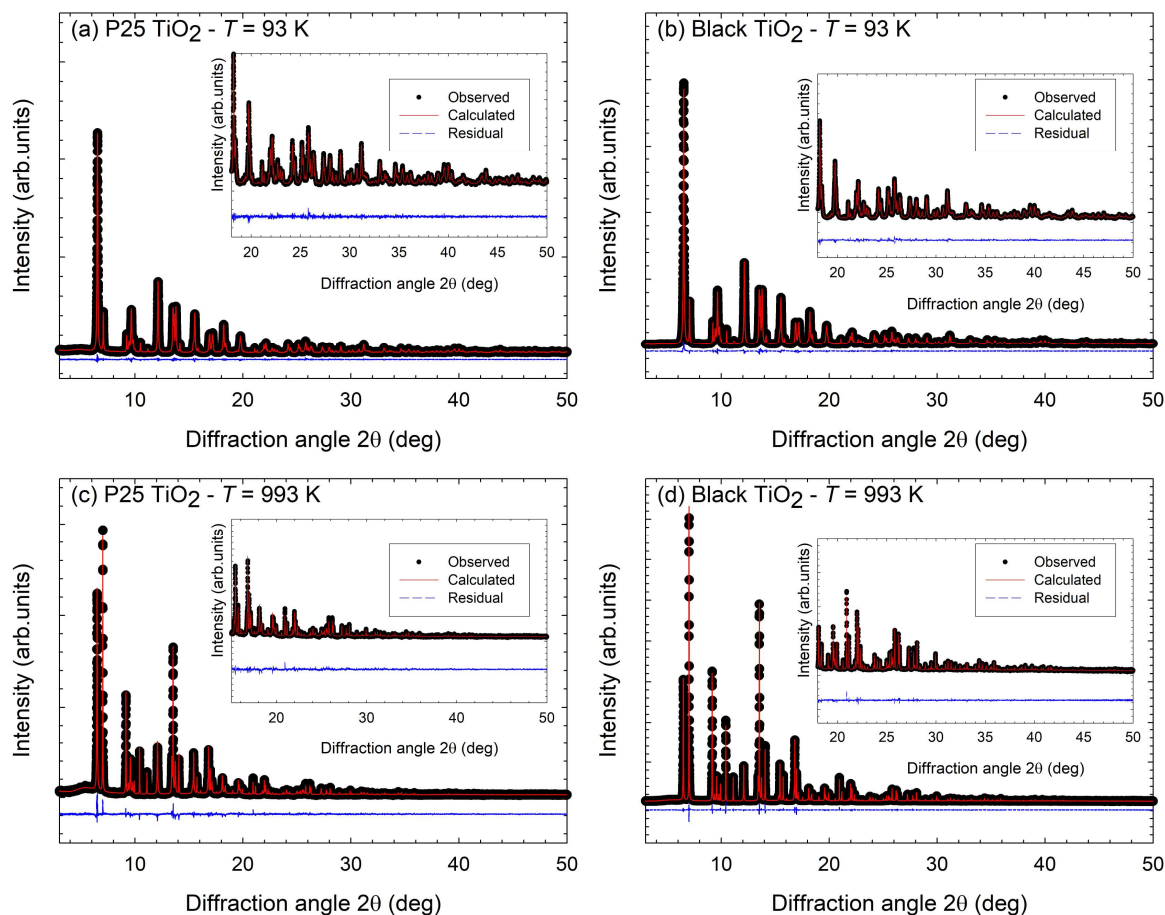


Figure 1. (a–d) Measured (dots) and calculated (lines) powder diffraction patterns for P25 and black TiO_2 at $T = 93$ K and $T = 993$ K, respectively. The inset shows a magnified view of the high angle diffraction peaks. The difference between the observed and fitted patterns is displayed at the bottom of each figure.

The transformation of anatase to rutile in TiO_2 does not occur at a unique T and has been a matter of debate for decades [9,10]. The reported transition temperatures range from 673 K to 1573 K, with the general consensus placing the transition around 873 K in pure bulk anatase under atmospheric conditions [9]. Several factors influence the transition temperature, including the size of the particles, the presence of dopants, as well as structural defects [9].

In this context, the temperature evolution of particle size D is shown in Figure 2b. At $T = 93$ K, the P25 and black anatase samples show really similar $D \sim 30$ nm, whereas an increase in size for black rutile $D \sim 62$ nm is observed in respect of the P25 rutile sample ($D \sim 62$ nm). At the transition, all the samples show an exponential increase in the particle size reaching $D \sim 43$ nm and $D \sim 85$ nm for anatase in the P25 and black samples. The rutile phase at $T = 993$ K displays $D \sim 85$ nm and $D \sim 110$ nm for P25 and black TiO_2 , respectively.

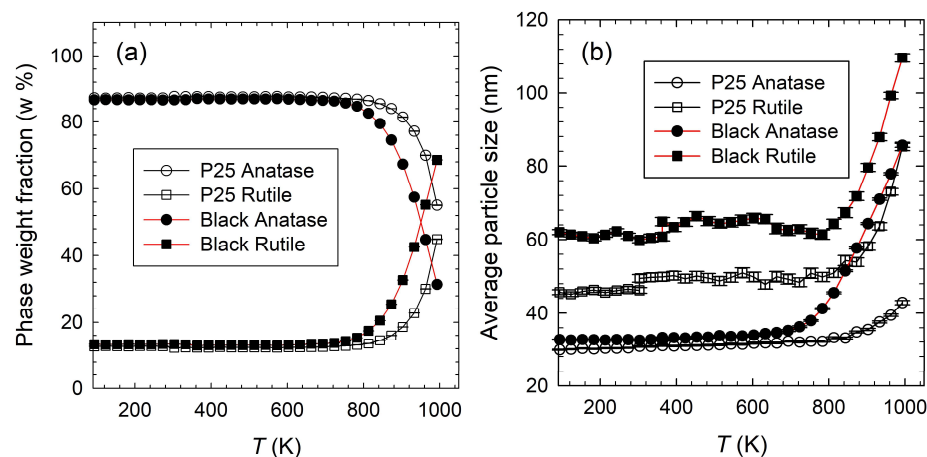


Figure 2. (a) Temperature evolution of anatase and rutile phase weight fraction for P25 and black TiO₂. (b) Average particle size (nm) estimation as a function of T . The lines are guides for the eye.

The anatase-to-rutile transformation is a thermodynamically driven process where the more stable rutile phase forms at the expense of the metastable anatase phase through a so-called reconstructive mechanism [9,21]. This transition involves the breaking of seven out of the twenty-four Ti-O bonds per unit cell of anatase, which requires overcoming a significant energy barrier. Above the transition temperature, the thermal energy is high enough to overcome the energy barriers for diffusion and surface energy reduction. This energy facilitates the movement of atoms or ions, allowing them to rearrange into the more thermodynamically stable rutile structure. The increased atomic mobility leads to the faster growth of the rutile particle size. Our observation of an almost exponential increase in particle size above the transition temperature can be explained by several factors related to the nature of the phase transformation and the kinetics involved. It is widely reported that commercial P25 TiO₂ powder contains small rutile crystallites interwoven with anatase [22]. This arrangement leads to an interface between the two forms of crystallites where at the transition temperature, small rutile nuclei form within the anatase matrix. As the temperature increases, these rutile nuclei grow at the expense of the anatase phase. Smaller particles tend to dissolve, and the material is redeposited onto larger particles integrating the pre-existing rutile. This phenomenon, known as Ostwald ripening, leads to an increase in the average particle size and can follow a kinetic profile that seems exponential under certain conditions [9,23]. The driving force for this process is the reduction in the total surface energy of the system. At higher T , sintering can also occur, where particles may fuse together to lower the total surface area, thus reducing the system's overall energy leading to a significant growth in particle size. The rate of sintering is typically slow at lower T but it can increase rapidly as the temperature rises. Finally, with increasing T , the nucleation rate of new rutile particles decreases because the system is approaching a thermodynamically stable state with fewer nucleation sites. Consequently, the growth mechanism dominates over nucleation, leading to the enlargement of existing particles rather than the formation of new, smaller particles. At higher temperatures, atomic diffusion is accelerated, facilitating the transport of material and the growth of larger particles at the expense of smaller ones. Within this framework, it can be anticipated that the elimination of oxygen ions through the creation of oxygen vacancies may expedite the transition, offering room for the rearrangement of ion movements and further diminishing the energy required for phase change [12]. Moreover, the presence of oxygen defects at the crystallite interfaces serves as nucleation sites for the anatase phase transformation [10,12]. The oxygen vacancies that are peculiar to reduced black TiO₂ could facilitate a phase transformation at lower temperatures [12]. This mechanism elucidates the observed, approximate 120 K discrepancy in the transition temperatures between two TiO₂ samples.

Further insights into the structural evolution are revealed by the temperature-dependent evolution of the unit cell parameters, as illustrated in Figure 3. In Figure 3a, both the *a*- and *c*-axis of anatase exhibit an almost linear thermal expansion behavior from RT up to 993 K. Both P25 and black TiO₂ nanoparticles follow a similar trend, indicating that the reduction process does not significantly affect the thermal expansion properties in the anatase phase. It is worth noting that the thermal expansion along the *c*-axis is less pronounced than the *a*-axis, which may be indicative of a weak anisotropic thermal evolution of anatase TiO₂ structure. Figure 3b demonstrates that both the *a*-axis and *c*-axis for the rutile phase of TiO₂ also exhibits a positive correlation with temperature, analogous to the anatase phase. Again, both P25 and black TiO₂ nanoparticles display a similar trend, suggesting the inherent thermal expansion characteristics of the rutile phase are maintained irrespective of H₂-reduced NPs. Figure 3c,d show the temperature evolution of the expansion coefficient α calculated for anatase and rutile in P25 and black samples, respectively. For both anatase P25 and black TiO₂, from 93 K to 400 K, all the thermal expansion coefficients display similar behavior and rather similar values. Above $T = 400$ K, the $\alpha_{a,T}$ coefficient is lower than for the *c*-axis, revealing a sort of anisotropic thermal expansion behavior. In the case of P25, $\alpha_{c,T}$ shows a step-like increase at about $T = 400$ K remaining relatively constant as the temperature approaches 1000 K. Black TiO₂ shows a more pronounced increase in $\alpha_{c,T}$ starting from around 600 K, suggesting that the anatase phase may undergo a precursor phenomenon related to the anatase-to-rutile structural transformation. On the other hand, the rutile phase (Figure 3d) shows somewhat constant thermal expansion coefficients across the measured temperature range, reflecting the linear T dependence of unit cell constants shown in Figure 3b.

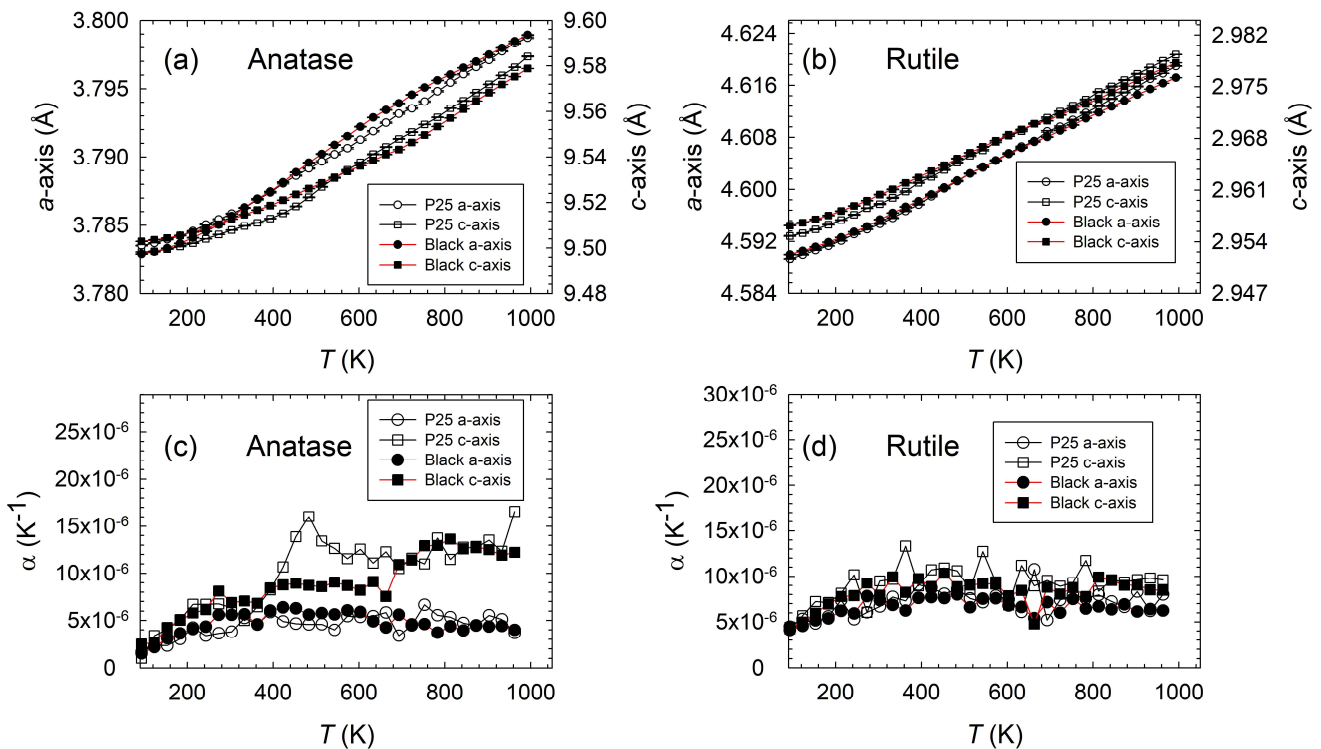
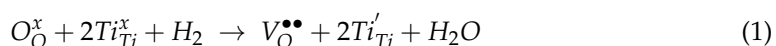


Figure 3. (a,b) Temperature evolution of *a*-axis and *c*-axis of P25 and black TiO₂ for anatase and rutile tetragonal phases, respectively. (c,d) Experimental coefficient of thermal expansion (α) of P25 and black TiO₂ for anatase and rutile tetragonal phases, respectively.

Our analysis presents a marked contrast to the findings of previous studies concerning the temperature dependence of the P25 anatase *c*-axis. Whereas prior studies have reported a pronounced non-linear behavior [10], characterized by a third-degree polynomial distribution up to 673 K followed by a sudden decrease beyond this transition temperature, our findings suggest a different behavior. In particular, these earlier observations pointed to a significant thermal expansion of the *c*-axis with increasing temperature, culminating in an estimated thermal expansion coefficient $\alpha_c \sim -1.5 \times 10^{-5} \text{ K}^{-1}$ within the temperature range of 773 K to 873 K [10]. This behavior was indicative of a strong negative thermal expansion (NTE), which contrasted sharply with our observations of relatively constant positive thermal expansion coefficients across a similar temperature range for both P25 and black TiO₂. Moreover, the reported NTE is typically associated with unique electronic and magnetic properties, often linked to changes in band structure and localized electron behaviors of materials contracting upon heating. Such changes can affect the material electronic transport properties and its response to external electric fields, leading to exotic physical phenomena like spin-lattice coupling, magnetic frustration, and magnetostriction. However, to the best of our knowledge, such properties have not been observed in undoped anatase nanostructured TiO₂, suggesting that NTE is not expected for these materials. Our findings thus emphasize a linear thermal expansion behavior in contrast to the complex non-linear dynamics reported previously [10].

From the structural perspective, the main difference between P25 and black is attributed to the formation of point defects. These defects are sensitively generated through H₂ reduction, as described by the following relation in Kröger–Vink notation [24]:



where $V_O^{\bullet\bullet}$ represents the oxygen vacancies and Ti'_{Ti} represents the electrons trapped at Ti⁴⁺ lattice sites.

Defect formation leads to the expansion and contraction of the lattice in the black sample, a phenomenon that has recently been elucidated by Santara et al. [25]. In their study on undoped, reduced rutile nanomaterials, the lattice expansion is caused by $V_O^{\bullet\bullet}$, which results from the relaxation of Ti-O interatomic distances and the interaction between $V_O^{\bullet\bullet}$ and Ti'_{Ti} . On the other hand, lattice contraction is driven by the Coulombic attraction between defects at the interstitial positions, e.g., O_i and Ti_i [25]. In addition, as already mentioned above, the presence of $V_O^{\bullet\bullet}$ is involved in promoting the anatase-to-rutile phase transformation due to the removal of oxygen ions which tailors in the reconstruction of Ti-O bonds. This reduces the phase-change energy which must be overcome before rearrangement of the structure can occur.

In this context, the nature of defects caused by the reduction process can then be inferred directly from the temperature evolution of Ti-O distances related to anatase and rutile phases. In Figure 4a,b, we present the temperature evolution of Ti-O to investigate the role of structural defects across the transition. The structural order in each phase is depicted in Figure 5 and consists of TiO₆ octahedra sharing four edges in anatase and two in rutile constituted of O ions at its vertices and Ti atoms at the center resulting in four short Ti-O (Ti-O basal) and two long Ti-O (Ti-O apical) distances.

For anatase in both P25 and black samples, the linear increase in both the apical and basal Ti-O interatomic distances with *T* suggests a uniform thermal expansion (see Figure 4a). The P25 sample shows a very similar expansion behavior to the black TiO₂ sample. This could be indicative of the fact that the intrinsic structural differences due to lattice defects in black sample cannot affect the *T* evolution of TiO₆ units in anatase structure.

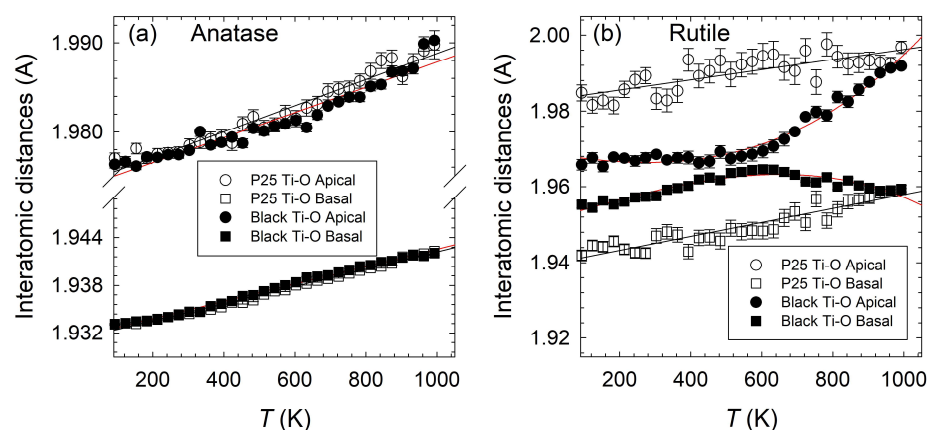


Figure 4. (a,b) Temperature evolution of Ti-O apical (circles) and Ti-O basal (squares) interatomic distances for anatase and rutile, respectively. Empty and full symbols are data related to P25 and black TiO₂ samples. The lines are guides for the eye.

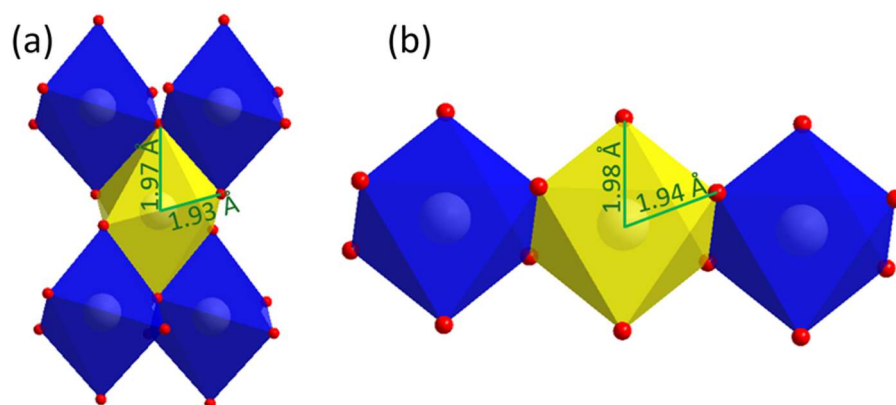


Figure 5. (a,b) Schematic TiO₆ octahedral units (blue) for anatase and rutile structures, respectively. Full chemical environment of a Ti octahedron is highlighted in yellow in both structures. Apical and basal Ti-O interatomic distances characteristic of the low temperature state of P25 are reported in the figure.

Conversely, the rutile form displays a more complex behavior (see Figure 4b). Basal and apical Ti-O distances in P25 exhibit a nearly linear behavior as a function of T , as observed in the anatase phase. The distances for the rutile black sample reveal a marked nonlinear increase with T indicating that the structure may undergo a strong reorientation of the crystal lattice associated with the modifications of H₂ reduction. At $T = 93$ K, the difference between apical and basal Ti-O is less pronounced than the P25 sample; however, we noted a significant expansion related to black Ti-O basal distances. According to the mechanism proposed by Santara et al. [25], this provides direct experimental evidence of the expansion expected from the $V_{\text{O}}^{\bullet\bullet}$ formation owing to the relaxation of Ti-O bonds around them. Above $T = 600$ K, the TiO₆ units become progressively more distorted and both the apical and basal Ti-O distances in black tend to values found for the P25 sample at $T \sim 900$ K.

This evolution can be even better appreciated considering the temperature dependence of the degree of distortion of TiO₆ octahedra (ϕ) for apical and basal Ti-O distances, which is defined as follows [16]:

$$\phi = \frac{Ti - O_{\text{apical}}}{Ti - O_{\text{basal}}} - 1 \quad (2)$$

Figure 6a illustrates the T evolution of the order parameter ϕ for both anatase and rutile. In the case of anatase, particularly for the P25 and black, ϕ exhibits a relatively stable trend across varying T , with minor fluctuations as the transformation temperature is approached. This pattern is also observed in the P25 sample for the rutile phase. The evolution of the ϕ parameter for black rutile is markedly complex. Initially, at lower temperatures, the ϕ parameter for black rutile starts at a minimal value of approximately 0.005. As the T increases, ϕ decreases, indicating a transition towards a regime where TiO_6 unit are more regular up to 600 K. Above this T , the ϕ parameter begins to increase, eventually aligning with the values observed for the P25 samples at the highest T (see Figure 6a).

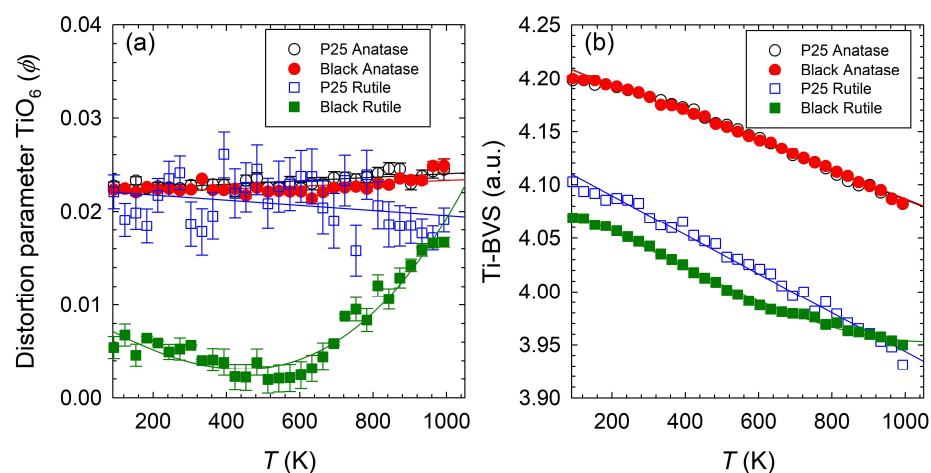


Figure 6. (a) Temperature evolution of degree of TiO_6 distortion (ϕ). (b) Bond valence sum (BVS) for Ti as a function temperature. Data are reported for anatase (circles) and rutile (squares) phases as determined in P25 and black TiO_2 . The lines are guides for the eye.

This analysis of the differences between anatase and rutile in P25 and black samples is markedly intriguing. It implies that the alterations triggered by H_2 significantly and principally impact the reduced structure of rutile. This suggests that the rutile TiO_2 is preferentially reduced over anatase through $V_{\text{O}}^{\bullet\bullet}$ and Ti'_{Ti} formation. To evaluate the reduction in rutile compared to anatase, we calculated the bond valence sum (BVS) [26,27] charges of Ti species from the experimental Ti-O using the tabulated parameters, i.e., $R_0 = 1.815 \text{ \AA}$ and $B = 0.37$ [28]. The results for all the samples are shown in Figure 6b. For all the nanocrystal phases, Ti-BVS decreases as T increases. This behavior agrees with the observed expansion of both apical and basal Ti-O, since, as suggested by Brown, the thermal expansion of the bond is assumed to be inversely related to the valence of the bond [26]. In other words, since the bond valence model is sensitive to interatomic distances (the valence of a bond decreases as the bond length increases), the BVS of Ti decreases as the Ti-O bond lengths would increase with T , reducing the electrostatic attraction between the Ti ions and O ions. For the anatase phase, both Ti-BVS share the same T evolution in the P25 and black samples. A clear depletion of Ti-BVS is evident in black rutile with respect to the P25 TiO_2 rutile. According to a recent study [29], this can be attributed to the differences in their atomic structure, bonding energies, and the electronic properties inherent to each phase. In particular, in the spatial arrangement surrounding black TiO_2 , the Ti atom deviates from the ideal octahedral, exhibiting four elongated basal bonds and two contracted bond lengths. Specifically, at the lowest temperature, the elongated basal bonds measure $\sim 1.96 \text{ \AA}$ in black rutile and $\sim 1.93 \text{ \AA}$ in anatase, while the apical bonds are $\sim 1.97 \text{ \AA}$ and $\sim 1.98 \text{ \AA}$, respectively. This indicates a more pronounced elongation in rutile, suggesting its bonds or bonding energy are comparatively weaker, thus requiring less energy for bond disruption. In addition, a recent study showed a lower charge density around the Ti atoms than the O atoms in reduced rutile, with the majority of Ti charge

density proximal to its adjacent O [29]. In anatase, the electron distribution between Ti and O showed uniformity, signifying isotropic bonding [29]. In rutile, electron clouds favor proximity to one of three Ti atoms, leading to a diminished covalent bond overlap and, hence, weaker Ti-O bonds. This insight into weaker covalent bonding in rutile aligns with the remarkable elongation of basal rutile Ti-O bonds observed here and the relative, reduced Ti valence as evidenced by BVS calculation (see Figure 6b).

Looking at the evolution of Ti-O distances on the black rutile, we observed an interesting behavior above $T \sim 600$ K—the disparity between basal and apical Ti-O distances begins to widen. This phenomenon, notable around $T = 123$ K beneath the transformation temperature, is likely a result of mechanisms activated during the transition from anatase to rutile. The formation of $V_{\text{O}}^{\bullet\bullet}$ in reduced rutile plays a crucial role in this context. We suggest that the phenomena observed may be attributed to the enhanced mobility of defects or the partial healing of $V_{\text{O}}^{\bullet\bullet}$ (filling by O_2) promoting upon increasing $T > 600$ K. We argue that the ongoing filling-up of the $V_{\text{O}}^{\bullet\bullet}$ disrupts the uniformity between the apical and the expanded basal Ti-O distances which are directly tied to the presence of lattice defects. Furthermore, our observations indicate that, beyond the transformation temperature of 900 K, the Ti-O distances in black rutile agree with those found in the P25 sample. This alignment strongly supports the Ostwald ripening proposed above, implying that the formation of a new, defect-free rutile lattice is notably enhanced by merging with an existing defective structure. Finally, we assume that the interactions of $V_{\text{O}}^{\bullet\bullet}$ with potential carbon atom sources present as impurities or from atmospheric CO_2 are negligible. This assumption is fully supported by the fact that during heating in air, the predominantly reduced material, the rutile phase of black TiO_2 , achieved at the higher T a degree of distortion comparable to that seen in the fully oxygenated rutile belonging to the P25 sample (see Figure 5a).

4. Conclusions

In this work, to summarize, we utilized in situ high-resolution synchrotron powder diffraction to conduct a detailed analysis of the thermal anatase-to-rutile phase transformation. By examining data from P25 and reduced black TiO_2 , we identified the role of oxygen vacancies in this phase transition without involving doping elements and other external factors. Our findings confirmed that the presence of pre-existing rutile facilitates the nucleation of the new phase, with oxygen vacancies aiding the reconstruction of Ti-O bonds, thereby enabling the transformation at T lower than those required for pure anatase. Our analysis clearly showed in both samples the almost linear T dependence of unit cell parameters effectively resolving the previously reported ambiguity regarding negative thermal expansion along the anatase c -axis [10]. The systematic study of the temperature-dependent evolution of Ti-O distances within the TiO_6 structural units distinctly indicates a preference for the reduction in the rutile phase over anatase in the black sample. Above 600 K, we discovered a novel structural regime in which the thermal dependency of basal and apical Ti-O bonds in rutile can be attributed to the partial reoccupation of oxygen vacancies. Importantly, the thermally induced filling of oxygen vacancies emerges as a critical phenomenon that may influence the photocatalytic properties of TiO_2 . In particular, oxygen vacancies serve as electron donors, enhancing the material's conductivity by contributing free carriers (electrons) to the conduction band upon thermal treatment. The reintegration of oxygen atoms into the lattice, however, may reduce the number of free carriers, potentially affecting TiO_2 conductivity and, consequently, its catalytic effectiveness by decreasing the number of active sites. Thus, understanding the complex interplay between the anatase-to-rutile phase transformation and oxygen vacancies offers valuable insights into designing efficient black materials with enhanced catalytic properties.

Author Contributions: Conceptualization, M.A. and A.N.; methodology, M.A., M.C. and A.N.; software, M.A. and M.C.; validation, M.A., M.C. and A.N.; formal analysis, M.A. and M.C.; investigation, M.A., M.C. and A.N.; resources, M.A. and A.N.; data curation, M.A. and M.C.; writing—original draft preparation, M.A.; writing—review and editing, M.A., M.C. and A.N.; visualization, M.A., M.C.

and A.N.; supervision, A.N.; project administration, A.N.; funding acquisition, A.N. All authors have read and agreed to the published version of the manuscript.

Funding: This research received no external funding.

Institutional Review Board Statement: Not applicable.

Informed Consent Statement: Not applicable.

Data Availability Statement: The data provided in this study are available upon request from the corresponding author.

Acknowledgments: The authors gratefully acknowledge the European Synchrotron Radiation Facility for provision of beam time and Andy Fitch for assistance in using the beamline (former ID31).

Conflicts of Interest: The authors declare no conflicts of interest.

References

1. Chen, X.; Mao, S.S. Titanium dioxide nanomaterials: Synthesis, properties, modifications, and applications. *Chem. Rev.* **2007**, *107*, 2891–2959. [[CrossRef](#)] [[PubMed](#)]
2. Ali, I.; Suhail, M.; Alothman, Z.A.; Alwarthan, A. Recent advances in syntheses, properties and applications of TiO₂ nanostructures. *RSC Adv.* **2018**, *8*, 30125–30147. [[CrossRef](#)] [[PubMed](#)]
3. Chen, X.; Liu, L.; Yu, P.Y.; Mao, S.S. Increasing solar absorption for photocatalysis with black hydrogenated titanium dioxide nanocrystals. *Science* **2011**, *331*, 746–750. [[CrossRef](#)] [[PubMed](#)]
4. Naldoni, A.; Allieta, M.; Santangelo, S.; Marelli, M.; Fabbri, F.; Cappelli, S.; Bianchi, C.L.; Psaro, R.; Santo, V.D. Effect of Nature and Location of Defects on Bandgap Narrowing in Black TiO₂ Nanoparticles. *J. Am. Chem. Soc.* **2012**, *134*, 7600. [[CrossRef](#)] [[PubMed](#)]
5. Xia, T.; Chen, X. Revealing the structural properties of hydrogenated black TiO₂ nanocrystals. *J. Mater. Chem. A* **2013**, *1*, 2983. [[CrossRef](#)]
6. Chen, X.; Liu, L.; Huang, F. Black titanium dioxide (TiO₂) nanomaterials. *Chem. Soc. Rev.* **2015**, *44*, 1861–1885. [[CrossRef](#)] [[PubMed](#)]
7. Liao, L.; Wang, M.; Li, Z.; Wang, X.; Zhou, W. Recent Advances in Black TiO₂ Nanomaterials for Solar Energy Conversion. *Nanomaterials* **2023**, *13*, 468. [[CrossRef](#)]
8. Howard, C.; Sabine, T.; Dickson, F. Structural and thermal parameters for rutile and anatase. *Acta Crystallogr. Sect. B Struct. Sci.* **1991**, *47*, 462–468. [[CrossRef](#)]
9. Hanaor, D.A.H.; Sorrell, C.C. Review of the anatase to rutile phase transformation. *J. Mater. Sci.* **2011**, *46*, 855–874. [[CrossRef](#)]
10. Kohobhange, S.P.; Karunadasa, C.H. Manoranjan Microstructural view of anatase to rutile phase transformation examined by in-situ high-temperature X-ray powder diffraction. *J. Solid State Chem.* **2022**, *314*, 123377.
11. Maqbool, Q.; Favoni, O.; Wicht, T.; Lasemi, N.; Sabbatini, S.; Stöger-Pollach, M.; Ruello, M.L.; Tittarelli, F.; Rupprechter, G. Highly Stable Self-Cleaning Paints Based on Waste-Valorized PNC-Doped TiO₂ Nanoparticles. *ACS Catal.* **2024**, *14*, 4820–4834. [[CrossRef](#)] [[PubMed](#)]
12. Tian, Z.; Du, S.; Cheng, X.; Zhang, J.; Li, F.; Chen, Z.; Lv, Y.; Zhu, Y.; Liu, G. The Role of Oxygen Vacancy in Anatase to Rutile Transformation of TiO₂. *Cryst. Growth Des.* **2022**, *22*, 6852–6856. [[CrossRef](#)]
13. Shi, T.; Duan, Y.; Lv, K.; Hu, Z.; Li, Q.; Li, M.; Li, X. Photocatalytic Oxidation of Acetone Over High Thermally Stable TiO₂ Nanosheets with Exposed (001) Facets. *Front. Chem.* **2018**, *6*, 175. [[CrossRef](#)] [[PubMed](#)]
14. Hummer, D.R.; Heaney, P.J.; Post, J.E. Thermal expansion of anatase and rutile between 300 and 575 K using synchrotron powder X-ray diffraction. *Powder Diffr.* **2007**, *22*, 352–357. [[CrossRef](#)]
15. Jagtap, N.; Bhagwat, M.; Awati, P.; Ramaswamy, V. Characterization of nanocrystalline anatase titania: An in situ HTXRD study. *Thermochim. Acta* **2005**, *427*, 37–41. [[CrossRef](#)]
16. Allieta, M.; Beranová, K.; Marelli, M.; Coduri, M.; Stefan, M.; Ghica, D.; Morello, G.; Malara, F.; Naldoni, A. Electron Small Polaron and Magnetic Interactions Direct Anisotropic Growth of Silicon-Doped Hematite Nanocrystals. *Cryst. Growth Des.* **2020**, *20*, 4719–4730. [[CrossRef](#)]
17. Dejoie, C.; Coduri, M.; Petitdemange, S.; Giacobbe, C.; Covacci, E.; Grimaldi, O.; Autran, P.-O.; Mogodi, M.W.; Jung, D.Š.; Fitch, A. Combining a nine-crystal multi-analyser stage with a two-dimensional detector for high-resolution powder X-ray diffraction. *J. Appl. Crystallogr.* **2018**, *51*, 1721–1733. [[CrossRef](#)]
18. Larson, A.C.; Von Dreele, R.B. *General Structure Analysis System (GSAS)*; Report LAUR 86-748; Los Alamos National Laboratory: Los Alamos, NM, USA, 2004.
19. Burdett, J.K.; Hughbanks, T.; Miller, G.J.; Richardson, J.W., Jr.; Smith, J.V. Structural-electronic relationships in inorganic solids: Powder neutron diffraction studies of the rutile and anatase polymorphs of titanium dioxide at 15 and 295 K. *J. Am. Chem. Soc.* **1987**, *109*, 3639. [[CrossRef](#)]
20. Gonschorek, W.F.; Feld, R. Neutron diffraction study of the thermal and oxygen position parameters in rutile. *Zeitschrift. fuer Kristallographie* **1982**, *161*, 1. [[CrossRef](#)]

21. Batzill, M.; Morales, E.H.; Diebold, U. Influence of nitrogen doping on the defect formation and surface properties of TiO₂ rutile and anatase. *Phys. Rev. Lett.* **2006**, *96*, 026103. [[CrossRef](#)]
22. Zhu, S.C.; Xie, S.H.; Liu, Z.P. Nature of rutile nuclei in anatase-to-rutile phase transition. *J. Am. Chem. Soc.* **2015**, *137*, 11532–11539. [[CrossRef](#)] [[PubMed](#)]
23. Chen, C.; Wang, Z.-Y. Synthesis and Crystal Growth Mechanism of Titanium Dioxide Nanorods. *J. Inorg. Mater.* **2012**, *27*, 45–48. [[CrossRef](#)]
24. Kro, F.A.; Vink, H.J. Relations between Concentrations of Imperfections in Crystalline Solids. *Solid State Phys.* **1956**, *3*, 307.
25. Santara, B.; Giri, P.K.; Imakita, K.; Fujii, M. Microscopic origin of lattice contraction and expansion in undoped rutile TiO₂ nanostructures. *J. Phys. D Appl. Phys.* **2014**, *47*, 215302. [[CrossRef](#)]
26. Brown, I.D. *The Chemical Bond in Inorganic Chemistry: The Bond Valence Model*; Oxford University Press: Oxford, UK, 2016.
27. Brown, I.D. Bond valence methods. In *Computer Modeling in Inorganic Crystallography*; Elsevier: Amsterdam, The Netherlands, 1997; pp. 23–53. [[CrossRef](#)]
28. Brown, I.D. Available online: <https://www.iucr.org/resources/data/datasets/bond-valence-parameters> (accessed on 17 March 2024).
29. Xu, J.; Huang, J.; Zhang, S.; Hong, Z.; Huang, F. Understanding the surface reduction of nano rutile and anatase: Selective breaking of Ti-O bonds. *Mater. Res. Bull.* **2020**, *121*, 110617. [[CrossRef](#)]

Disclaimer/Publisher's Note: The statements, opinions and data contained in all publications are solely those of the individual author(s) and contributor(s) and not of MDPI and/or the editor(s). MDPI and/or the editor(s) disclaim responsibility for any injury to people or property resulting from any ideas, methods, instructions or products referred to in the content.